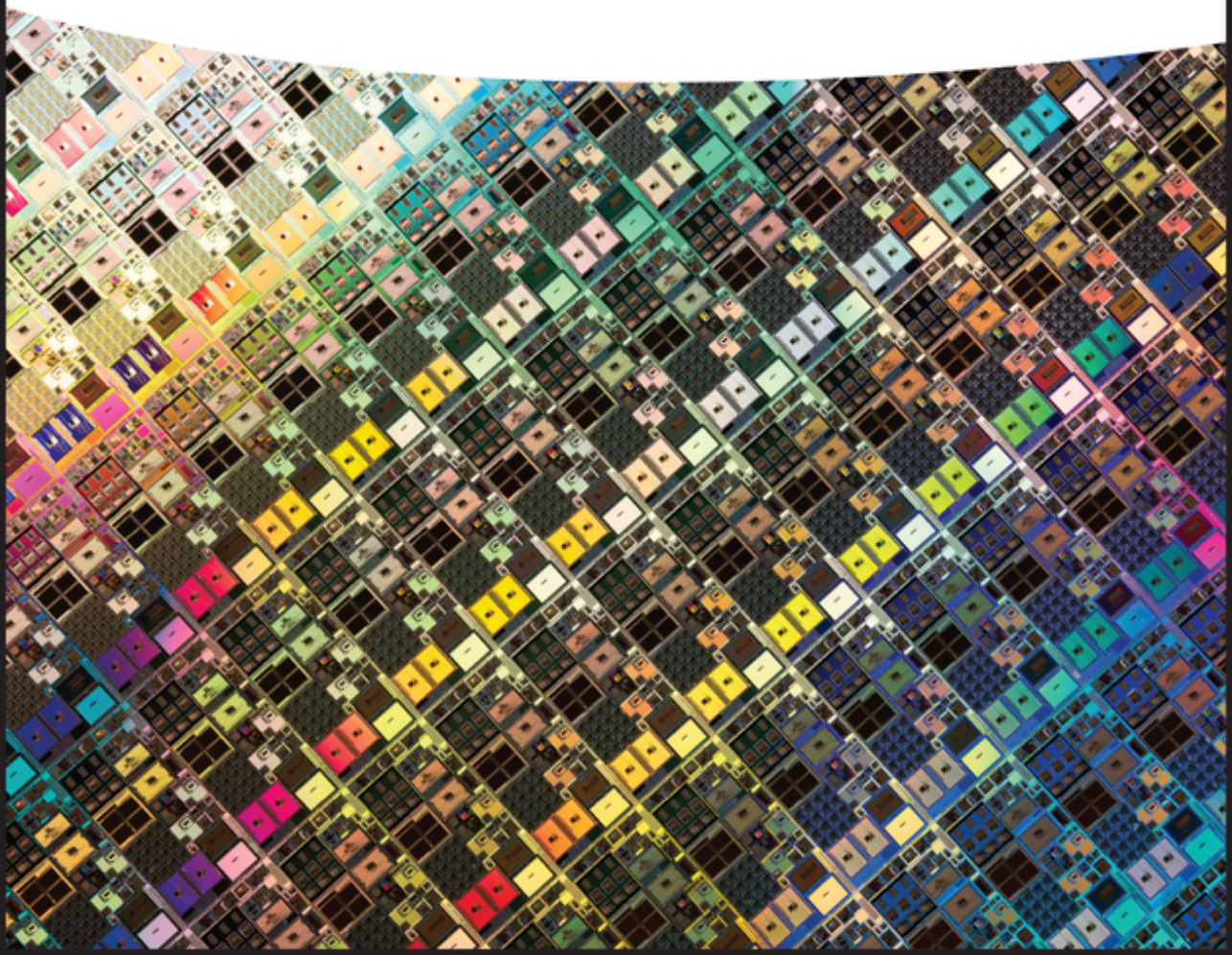


WILEY-VCH

Edited by Visakh P.M., Artem Semkin,  
Raneesh Balakrishnan, and Saša Lazović

# Nanotechnology in Electronics

Materials, Properties, Devices





## **Nanotechnology in Electronics**



# **Nanotechnology in Electronics**

Materials, Properties, Devices

*Edited by Visakh P.M., Artem Semkin, Raneesh Balakrishnan,  
and Saša Lazović*

**WILEY-VCH**

## Editors

### ***Dr. Visakh P.M.***

Department of Physical Electronics  
TUSUR University  
Lenin Avenue 30  
634050 Tomsk  
Russia

### ***Dr. Artem Semkin***

TUSUR University  
Department of Microwave and Quantum  
Radio Engineering, TUSUR University  
Lenin Avenue 30  
634050 Tomsk  
Russia

### ***Dr. Raneesh Balakrishnan***

Department of Physics  
Catholicate College  
Pathanamthitta  
689645, Kerala  
India

### ***Dr. Saša Lazović***

Biomimetics Laboratory  
Innovation Center, Institute of Physics  
Belgrade  
Pregrevica 118  
11080 Belgrade  
Serbia

**Cover Image:** © MirageC/Getty Images

■ All books published by **WILEY-VCH** are carefully produced. Nevertheless, authors, editors, and publisher do not warrant the information contained in these books, including this book, to be free of errors. Readers are advised to keep in mind that statements, data, illustrations, procedural details or other items may inadvertently be inaccurate.

**Library of Congress Card No.:**  
applied for

**British Library Cataloguing-in-Publication Data**  
A catalogue record for this book is available from the British Library.

### **Bibliographic information published by the Deutsche Nationalbibliothek**

The Deutsche Nationalbibliothek lists this publication in the Deutsche Nationalbibliografie; detailed bibliographic data are available on the Internet at <<http://dnb.d-nb.de>>.

© 2023 WILEY-VCH GmbH, Boschstraße 12,  
69469 Weinheim, Germany

All rights reserved (including those of translation into other languages). No part of this book may be reproduced in any form – by photoprinting, microfilm, or any other means – nor transmitted or translated into a machine language without written permission from the publishers. Registered names, trademarks, etc. used in this book, even when not specifically marked as such, are not to be considered unprotected by law.

**Print ISBN:** 978-3-527-34673-8

**ePDF ISBN:** 978-3-527-82421-2

**ePub ISBN:** 978-3-527-82423-6

**oBook ISBN:** 978-3-527-82422-9

**Typesetting** Straive, Chennai, India

## Contents

**Preface** *xiii*

- 1 Nanotechnology in Electronics, Materials Properties, and Devices: State of the Art and Future Challenges** *1*  
*P. M. Visakh and Raneesh Balakrishnan*
- 1.1 Graphene-based Nanoelectronic Biosensors *1*
- 1.2 Zinc Oxide Piezoelectric Nanogenerators for Low-frequency Applications *2*
- 1.3 Investigation of the Hot Carrier-induced Degradation in Nanoscale Junctionless MOSFETs: A Reliability-based Analysis *3*
- 1.4 Study of Electrostatic and Dispersion Forces in Nanoelectromechanical Systems (NEMS) *4*
- 1.5 Nanomaterials for Wearable, Flexible, and Stretchable Strain/Pressure Sensors *5*
- 1.6 Conductive Nanomaterials for Printed and Flexible Electronics Application *6*
- 1.7 Metal-oxide Semiconductors for Noninvasive Diagnosis of Breast Cancer *8*
- 1.8 Down-conversion Photoluminescence Properties of  $\text{ZrO}_2: \text{Ln}^{3+}$  (Ln = Eu, Sm, Er, Tb, Ho, Tm, Pr, Gd, Dy) Films Formed by Plasma Electrolytic Oxidation *10*
- 1.9 Multiferroics for Spintronic Applications *10*
- 1.10 Quartz Tuning Fork Based Nanosensors *12*
- References *13*
- 2 Graphene-based Nanoelectronic Biosensors** *25*  
*Muhammad Aamir, Ahmed Shuja, Saba Ashraf, and Javeed Akhtar*
- 2.1 Introduction on Graphene *25*
- 2.2 History of Graphene *26*
- 2.3 Properties of Graphene *27*
- 2.4 Fundamentals of G-Derivatives *27*
- 2.5 Synthesis of Graphene *28*
- 2.5.1 Graphene-based Nanoelectronics *30*

2.5.2	Graphene-based Biosensors	32
2.5.3	Graphene in Electrochemical Biosensing Platforms	33
2.5.4	Field-effect Transistors	34
2.5.5	Optical Platform for Biosensing	34
2.6	Applications of Graphene-based Biosensors	35
2.6.1	Graphene-based Electrochemical Biosensors	35
2.6.2	Detection of Acute Myocardial Infarction	36
2.6.3	Detection of Lung Cancer	37
2.6.4	Detection of Asthma	37
2.6.5	Detection of Diabetes	38
2.6.5.1	Electrochemical Enzymatic Glucose Biosensor	38
2.6.5.2	Nonenzymatic Glucose Biosensors	40
2.6.6	Detection of Cholesterol	41
2.6.6.1	Enzymatic Detection of Cholesterol	41
2.6.6.2	Enzyme-free Biocatalytic Oxidation of Cholesterol	41
2.6.7	Detection of Hydrogen Peroxide	42
2.6.8	Hydrogen Peroxide Detection in Living Cells	43
2.6.9	Nucleic Acid Biosensors	43
2.6.10	Detection of Enzymes	44
2.6.11	Food Toxin Sensing	45
2.6.12	Heavy Metal Detection	45
2.6.13	Detection of Pesticides	45
2.6.14	Graphene-based Fluorescent Biosensors	46
2.6.15	Detection of Small Molecules	46
2.6.16	Detection of Nucleic Acids	47
2.6.17	Detection of Pathogens and Food Toxins	47
2.6.18	Detection of Toxic Heavy Metal Ions	47
	References	48
<b>3</b>	<b>Zinc Oxide Piezoelectric Nanogenerators for Low-frequency Applications</b>	<b>63</b>
	<i>Zohreh Moarref, Negar Honaramiz Fahim, and Majid Montazer</i>	
3.1	Introduction of Zinc Oxide	63
3.1.1	Structure of ZnO NPs	63
3.1.2	Crystal Structure of ZnO NPs	63
3.1.3	Methods for Synthesis of ZnO NPs	66
3.1.3.1	Mechanochemical Methods	66
3.1.3.2	Sol-gel Synthesis	66
3.1.3.3	Hydrothermal Method	67
3.1.3.4	Liquid-phase Synthesis	67
3.1.3.5	Controlled Precipitation	67
3.1.3.6	Vapor Transport Synthesis	68
3.1.4	Piezoelectric Effect of ZnO	69
3.2	Zinc Oxide Piezoelectric Nanogenerators	70
3.2.1	Nanogenerators	71

3.2.1.1	Piezoelectric Nanogenerators (PENGs)	71
3.2.1.2	Triboelectric Nanogenerators (TENGs)	73
3.2.1.3	Pyroelectric Nanogenerators	74
3.2.1.4	Hybrid Nanogenerators	75
3.2.2	Zinc Oxide Piezoelectric Nanogenerators	76
3.3	Zinc Oxide Piezoelectric Nanogenerators for Low-frequency Applications	79
3.3.1	Approaches for Scavenging Low-frequency Vibrations	79
3.3.2	Device Structures	79
3.3.2.1	Arc Shaped	79
3.3.2.2	Cantilever	80
	Conclusion	85
	References	86
<b>4</b>	<b>Investigation of Hot Carrier–induced Degradation in Nanoscale Junctionless MOSFETs: A Reliability-based Analysis</b>	<b>97</b>
	<i>Nidhal Abdelmalek, Fayçal Djeffal, and Toufik Bentrchia</i>	
4.1	Introduction	97
4.2	Overview of the Junctionless Paradigm	98
4.3	Simulation Framework of Hot Carrier Degradation	102
4.4	Creation of Interface Traps	104
4.5	Performance Degradation Due to Hot Carrier Effect	108
4.6	Hot Carrier Degradation in Digital Applications	118
4.6.1	Static Analysis	118
4.6.2	Transient Analysis	119
4.7	Concluding Remarks	122
	References	122
<b>5</b>	<b>Study of Electrostatic and Dispersion Forces in Nanoelectromechanical Systems (NEMS)</b>	<b>127</b>
	<i>Masoud SoltanRezaee and Amin Farrokhhabadi</i>	
5.1	Introduction	127
5.2	Electrostatic Forces	131
5.2.1	Rectangular Beam–Plate	131
5.2.2	Wire–Plate	131
5.2.3	Carbon Nanotube (CNT) Sheets	132
5.2.4	Rectangular Tweezers	132
5.2.5	Carbon Nanotube (CNT) Tweezers	134
5.3	Fringing Field Effects	135
5.3.1	Palmer’s Model	136
5.3.2	Mejjs–Fokkema Model	136
5.3.3	Other Models	136
5.4	Van der Waals Force	137
5.5	Rectangular Beam–Sheets	138

- 5.5.1 Wire–Plate 138
- 5.5.2 Carbon Nanotube (CNT) Sheets 138
- 5.5.3 Rectangular Tweezers 139
- 5.5.4 Circular Tweezers 140
- 5.5.5 Carbon Nanotube (CNT) Tweezers 140
- 5.6 Casimir Force 141
- 5.6.1 Rectangular Beam–Plate 142
- 5.6.2 Wire–Plate 142
- 5.6.3 Carbon Nanotube (CNT) Sheets 143
- 5.6.4 Rectangular Tweezers 143
- 5.6.5 Circular Tweezers 143
- 5.6.6 Carbon Nanotube (CNT) Tweezers 144
- 5.7 Other Theories Related to the Casimir Force 144
- 5.7.1 Proximity Force Approximation (PFA) 144
- 5.7.2 Dirichlet and Neumann Modes 148
- 5.8 Freestanding Phenomenon 149
- 5.8.1 Detachment Length 149
- 5.8.2 Surface Layer and Size-dependent Effects 150
- 5.9 Summary 151
- References 151
  
- 6 Nanomaterials for Wearable, Flexible, and Stretchable Strain/Pressure Sensors 155**  
*Ali Sedighi and Majid Montazer*
- 6.1 Introduction 155
- 6.2 Wearable Strain/Pressure Sensors 156
- 6.2.1 Piezoresistive Sensors 157
- 6.2.2 Capacitive Sensor 167
- 6.2.3 Piezoelectric Sensors 171
- 6.2.4 Triboelectric Sensors 173
- 6.3 Applications 174
- 6.3.1 Movement Monitoring and Daily Performance Tracking 174
- 6.3.2 Health Monitoring 176
- 6.3.3 Human–machine Interface, Soft Robotics, and Artificial Skin 178
- 6.4 Conclusion and Outlook 184
- References 185
  
- 7 Conductive Nanomaterials for Printed and Flexible Electronics Application 207**  
*K. Thiyagarajan, S.G. Rahul, G.K. Rajini, Debashis Maji, and Arunkumar Chandrasekhar*
- 7.1 Introduction 207
- 7.2 Printing Technology and Challenges with Fabrication of Electronics 208
- 7.2.1 Inkjet Printing 209

7.2.2	Screen Printing	210
7.2.3	Slot Die Coating	210
7.2.4	Electrohydrodynamic (EHD) Printing	211
7.2.5	Gravure Printing	211
7.2.6	Flexographic Printing	212
7.2.7	Roll-to-roll (R2R) Printing	212
7.2.8	Printable Nanomaterials Requirements	212
7.3	Synthesis and Preparation of Nanomaterial-based Inks	213
7.3.1	Metallic-based Inks	214
7.3.1.1	Silver Nanoparticles	215
7.3.1.2	Silver Nanowires	222
7.3.2	1D and 2D Material-based Inks	225
7.3.2.1	CNT Ink	225
7.3.2.2	Graphene Ink	228
7.4	Outlooks and Perspectives	235
	References	235

## **8 Metal-oxide Semiconductors for Noninvasive Diagnosis of Breast Cancer** 241

*Mohan Velumani, Ivneet Banga, Anirban Paul, Asokan Prasanth, Samir Ranjan Meher, Elizabeth Rufus, Sriram Muthukumar, Shalini Prasad, and Zachariah C. Alex*

8.1	Introduction	241
8.2	Sensing Material and Techniques	244
8.3	Biomarkers for Noninvasive Diagnosis of Breast Cancer	246
8.3.1	Body Metabolism for VOC Generation	247
8.3.2	Various Components of Human Breath and Its Related Diseases	249
8.3.3	Breast Cancer-related VOCs	250
8.4	Sensing Elements	251
8.4.1	Various Materials for VOC Sensing	251
8.4.2	Metal Oxides for VOC Sensing	252
8.4.3	Significance of Composite Metal Oxides	252
8.5	Fabrication Methods	252
8.5.1	Thin Film Deposition	252
8.5.1.1	Vacuum-based Techniques	254
8.5.1.2	Chemical Routes	254
8.5.2	Thick Film Deposition	255
8.5.3	Growth of Nanomaterials	255
8.5.3.1	Physical Methods	256
8.5.3.2	Chemical Methods	257
8.6	Noninvasive Techniques for Breast Cancer Diagnosis	257
8.6.1	Selected Ion Flow Tube Mass Spectrometry (SIFT-MS)	257
8.6.2	Proton Transfer Reaction Mass Spectrometry (PTR-MS)	258
8.6.3	Gas Chromatography–Mass Spectrometry (GC-MS)	258
8.6.4	Differential Mobility Spectrometer (DMS)	261

8.6.5	Chemiresistive Sensing Mechanism	261
8.6.6	Fiber-optic Sensors	262
8.6.6.1	Evanescent Wave Fiber-optic VOC Sensors	263
8.6.6.2	Lossy Mode Resonance Fiber-optic VOC Sensors	263
8.6.7	Surface Plasmon Resonance Sensor	264
8.6.8	Calorimetric Sensors	265
8.7	Conclusion	266
	Acknowledgements	266
	References	267

**9 Down-conversion Photoluminescence Properties of  $ZrO_2 : Ln^{3+}$  ( $Ln = Eu, Sm, Er, Tb, Ho, Tm, Pr, Gd, Dy$ ) Films Formed by Plasma Electrolytic Oxidation** 279

*Aleksandar Ćirić and Stevan Stojadinović*

9.1	Introduction	279
9.2	Experiment	280
9.3	Results and Discussion	281
9.3.1	Morphology, Chemical, and Phase Composition	281
9.3.2	PL of $ZrO_2$ Films	283
9.3.2.1	PL of Undoped $ZrO_2$	283
9.3.2.2	PL of $ZrO_2 : Eu^{3+}$	283
9.3.2.3	PL of $ZrO_2 : Sm^{3+}$	286
9.3.2.4	PL of $ZrO_2 : Er^{3+}$	286
9.3.2.5	PL of $ZrO_2 : Tb^{3+}$	287
9.3.2.6	PL of $ZrO_2 : Ho^{3+}$	288
9.3.2.7	PL of $ZrO_2 : Tm^{3+}$	288
9.3.2.8	PL of $ZrO_2 : Pr^{3+}$	290
9.3.2.9	PL of $ZrO_2 : Gd^{3+}$	292
9.3.2.10	PL of $ZrO_2 : Dy^{3+}$	292
9.4	CIE Chromaticity of $ZrO_2 : Ln^{3+}$	295
9.5	Conclusion	295
	Acknowledgments	296
	References	296

**10 Multiferroics for Spintronic Applications** 301

*Jini K. Jose and Raneesh Balakrishnan*

10.1	Magnetoelectric Multiferroic Materials	301
10.2	Spintronics	302
10.2.1	Fundamental Aspects of Spintronics	302
10.2.2	Giant Magnetoresistance	303
10.2.3	Tunneling Magnetoresistance	304
10.3	Spintronic Devices	305
10.3.1	Spin Valve	306
10.3.2	Multiferroic Tunnel Junctions	307
10.3.3	Spin FET	309

10.3.4	Spin LED	311
10.4	Summary	311
	References	312
<b>11</b>	<b>Quartz Tuning Fork–Based Nanosensors</b>	<b>317</b>
	<i>S. Abraham Sampson and Suwarna S. Datar</i>	
11.1	Introduction	317
11.2	Chemical Sensors	318
11.3	Quartz Tuning Forks (QTFs)	319
11.4	Early QTF Development	324
11.5	QTF as a Sensor	325
11.5.1	Mass-loaded QTFs as Sensors	328
11.5.2	Polymer Wire/Film Modified QTF Sensor	331
11.5.2.1	QTFs Modified with Polymer Wire Bridges	331
11.5.2.2	QTFs Modified with Polymer Film Bridges	338
11.5.2.3	Improving Selectivity of Polymer-modified QTF Sensors and Classification of VOCs	342
11.6	Conclusions	347
	References	351
	<b>Index</b>	<b>357</b>



## Preface

Nanotechnology is one of the most talked about technologies today. The application of nanotechnology in modern electronic devices, especially memory devices, nanoscale transistors, nanosensors, etc., improves the devices' functionalities. Not only is the power consumption in nanoelectronic devices reduced drastically but also the weight and thickness of the devices are decreased. This book summarizes recent research accomplishments in the area of nanotechnology-based electronics, its properties, and applications.

A brief description of the book content and an introduction to nanotechnology in electronics and current challenges are given in the first chapter. The second chapter offers a review of graphene-based nanoelectronic biosensors. This chapter covers the introduction to graphene, its properties, and some novel potential applications as biosensors. Zinc oxide piezoelectric nanogenerators for low-frequency applications are described in Chapter 3. Different types of ZnO nanostructure-based nanogenerators are discussed. Chapter 4 deals with the investigation of hot carrier-induced degradation in nanoscale junctionless MOSFETs. The fifth chapter discusses the electrostatic and dispersion forces in nano-electromechanical systems. In addition, the effects of different electric fringing field corrections and other effects related to the Casimir force are separately reported. The sixth chapter deals with nanomaterials that can be used as wearable, flexible, and stretchable strain/pressure sensors. A detailed review of conductive nanomaterials for printed and flexible electronics applications is covered in the seventh chapter, with the fundamentals, features, and progress in various printing technologies.

The application of different metal oxide semiconductors for the non-invasive diagnosis of breast cancer is discussed in Chapter 8. This review outlines breast cancer-related volatile organic compounds and the detection mechanisms currently used for diagnosis. The ninth chapter presents the down-conversion photoluminescence properties of  $\text{ZrO}_2:\text{Ln}^{3+}$  ( $\text{Ln} = \text{Eu}, \text{Sm}, \text{Er}, \text{Tb}, \text{Ho}, \text{Tm}, \text{Pr}, \text{Gd}, \text{Dy}$ ) films formed by plasma-electrolytic oxidation. Chapter 10 provides an overview of multiferroics for spintronics applications. This chapter reviews the fundamental aspects and applications of multiferroic-based spintronic devices. The eleventh chapter covers many of the latest research accomplishments in quartz tuning fork-based nanosensors.

In this book, chapter authors have reviewed different aspects of nanotechnology in the field of electronics and related advancements. This book is a valuable reference source for faculties, professionals, research fellows, senior graduate students, and researchers working in the field of nanotechnology/electronics. The use of nanomaterial in electronics is considered as a promising area of research, a lot of research activities are going on, and some knowledge of nanoelectronics is helpful to bring a change in the current techniques and applications. Finally, we would like to express our sincere gratitude to all the contributors of this book, who made excellent support to the successful completion of this venture. We also thank the publisher Wiley for recognizing the demand and importance of nanotechnology in the field of electronics.

*Visakh P.M.*

*Artem Semkin*

*Raneesh Balakrishnan*

*Saša Lazović*

## 1

## Nanotechnology in Electronics, Materials Properties, and Devices: State of the Art and Future Challenges

P. M. Visakh<sup>1</sup> and Raneesh Balakrishnan<sup>2</sup>

<sup>1</sup>Faculty of Electronic Engineering, Department of Physical Electronics, TUSUR University, Tomsk 634050, Russia

<sup>2</sup>Department of Physics, Catholicate College, Pathanamthitta, Kerala, 689645, India

### 1.1 Graphene-based Nanoelectronic Biosensors

Graphene is the thinnest, strongest material, with one-particle thickness, and is 200 times stronger than steel. Graphene exhibits outstanding electrical and thermal conductivity with remarkable light absorption capability. Graphene is a material that could change the world in the true sense, with its infinite potential for integration practically in any industry. Graphene has diverse forms and can be combined with other materials to form various materials of extraordinary characteristics. Researchers are very keen to explore and patent graphene and gain expertise about its various properties and potential applications, mainly in cells, transistors, computer chips, supercapacitors, energy production, etc.

The common graphene derivatives are pristine graphene, reduced graphene oxide, graphene quantum dots (GQDs), and polycrystalline graphene, which are extensively used in biosensing applications. Pristine graphene consists of single crystalline grains that have flawless lattices made up of defect-free hexagonal ring networks of  $sp^2$  hybridized carbon atoms [1]. Graphene oxide also mainly consists of covalently bonded  $sp^2$ -hybridized carbon atoms but has some defects due to the following reasons: disrupted  $sp^3$ -hybridized carbon atoms and the oxygen functional groups like carboxyl group located at the edges and the basal plane are saturated with hydroxyl and epoxy groups [2]. The presence of these groups makes graphene oxide hydrophilic depending on their oxidation state [3].

Nanoelectronic devices are made up of nanomaterials such as nanowires, graphene, carbon nanotubes (CNTs), and transition metal dichalcogenides. These nanomaterials must possess extraordinary characteristics such as high surface-area-to-volume ratio, low power consumption, high charge mobility, and excellent compatibility to fit in modern electronic devices. As nanomaterials display unusual properties that are not obtainable at the micro scale, nanoelectronics holds

significant importance. Graphene is a recently discovered nanomaterial known for its outstanding mechanical, electrical, and optical properties [4–6]. To develop an efficient graphene-based electrochemical biosensor, the graphene oxide nanosheets were decorated with Au NPs by aryldiazonium bridges fabricated on glassy carbon electrode (GCE). Then, the glucose oxidase enzyme was immobilized on the graphene oxide–Au NP nanocomposites. The biosensor showed a high sensitivity of about  $42 \mu\text{A mM}^{-1} \text{cm}^{-2}$  with a wide detection range of 0.3–20 mM. This glucose biosensor showed excellent selectivity for glucose detection [7].

N-doped graphene–chitosan–glucose oxidase biosensors showed an excellent sensitivity of  $226.24 \mu\text{A mM}^{-1} \text{M}^{-2} 120$  due to high porosity of graphene and high conductivity of graphene sheets, which facilitate enhanced electron transfer. The CuO nanoparticle (NP) composites with graphene oxide have shown a high sensitivity of  $262.52 \mu\text{A mM}^{-1} \text{cm}^{-2}$  with an LOD of  $0.69 \mu\text{M}$ . This biosensor was also used for human serum detection and showed a sensitivity of  $285.38 \mu\text{A mM}^{-1} \text{cm}^{-2}$  [8]. Similarly, biosensors based on Pt–NiO–reduced graphene oxide nanocomposites showed a sensitivity of  $832.95 \mu\text{A mM}^{-1} \text{cm}^{-2}$  and an LOD of  $2.67 \mu\text{M}$ . This high performance was attributed to porosity of Pt–NiO–reduced graphene oxide nanocomposites [9]. Moreover, the Cu–Co–reduced graphene oxide nanocomposites were electrochemically deposited over the pencil graphite electrode and showed a high sensitivity of  $240 \mu\text{A mM}^{-1} \text{cm}^{-2}$  and an LOD of  $0.15 \mu\text{M}$  [10].

## 1.2 Zinc Oxide Piezoelectric Nanogenerators for Low-frequency Applications

Nanoparticles can be fabricated through solid-phase, liquid-phase, and gas-phase methods. Chemical bath deposition [11], green chemistry synthesis [12], and wet chemical methods [13] are other recently used techniques for the synthesis of ZnO NPs. Vertical ZnO nanorods were grown hydrothermally on a gold-coated PTFE (polytetrafluoroethylene). Spin coating was used to deposit 0.005 M zinc acetate dehydrated in ethanol on the surface of gold-coated PTFE film. Then, the substrate was heated at  $90^\circ\text{C}$  for 30 minutes. The seed layer was uniformly deposited in a two-step process of deposition and decomposition to cover the substrate. ZnO nanorods were hydrothermally grown on the seed layer. Zinc nitrate hexahydrate and hexamethylenetetramine (HMT) were used to hold the seed layer at  $90^\circ\text{C}$  for three hours [14].

Masuda et al. [15] demonstrated a simple liquid-phase synthesis method to control the morphology and crystal size of ZnO. ZnO nanowires of 100 nm long and about 50 nm wide were successfully synthesized at  $50^\circ\text{C}$ . They also found that nanowires had no branches without aggregations. Several techniques have been explored to synthesize and develop both direct and alternating current zinc oxide piezoelectric nanogenerators [16]. Controlled precipitation is typically used to produce ZnO NPs in large quantities with reproducible properties for use in industrial products. In this process, zinc salt solution is spontaneously reduced by a reducing agent.

Breaking down of agglomerations is an important process in this method. Therefore, temperature, pH, type of aqueous media, time of precipitation, and the raw materials are most important parameters in the precipitation of ZnO NPs, which have impact on the size and final characteristics of the nanoparticles [17]. Aladpoosh et al. [18] used the ZnO-controlled precipitation method, a green synthesis method using natural plant source, namely, Keliab and zinc acetate. Wurtzite structure and nanorod shapes result from in situ synthesis of ZnO on the cellulosic chains of cotton using the green synthesis method. The principle of nanogenerators was first used by Wang's research group in 2006 [19]. They used a conductive tip of an atomic force microscope (AFM) to deflect the aligned semiconductor ZnO nanowires and successfully obtained a measurable piezoelectric voltage output of around 10 mV. They grew ZnO nanorods on a sapphire substrate using a vapor–liquid solid method, which caused the gold particles to remain on the top of each rod after their growth.

A Schottky contact was formed between the conductive AFM tip and the semiconductor ZnO nanowires, which is a key factor in current generation by piezoelectric nanogenerators. The stretched side of the rod with a positive potential produced a reverse bias with the Schottky junction, leading to no current to screen the polarization. When the contact between the tip and the compressed, negatively polarized side of the rod was disconnected, the junction was forward biased, and the current was able to flow and screen the polarization. Monitoring the open-circuit voltage reflects an uncertainty in the measurement of this type of device [20]. Zinc oxide is an environmentally friendly multifunctional semiconductor possessing outstanding piezoelectric effect, piezoelectric coupling coefficient, and thermal and mechanical stability at room temperature. Owing to its non-centrosymmetric hexagonal wurtzite crystal structure and polar Zn—O bonds, ZnO has unique piezoelectric properties as the core of studies in the ceramic industry [21, 22]. For the first time in 2009, Xi and coworkers [23] fabricated a ZnO-nanotube-based piezoelectric nanogenerator. They used a solution chemical method to synthesize hexagonal ZnO nanotube arrays at temperatures below 100 °C.

ZnO-based nanogenerators can be incorporated into various substrates. In 2012, Khan et al. [24] grew ZnO nanorods on a silver-coated cotton fabric using a low-temperature, aqueous chemical growth method. An external force was applied on ZnO nanorods via an AFM tip, where the flow of charges was taken into account and a Schottky barrier formed between the electrode and the nanorods.

### **1.3 Investigation of the Hot Carrier–induced Degradation in Nanoscale Junctionless MOSFETs: A Reliability-based Analysis**

In the past decades, reliability of MOSFET devices was a major concern in the electronics industry: the aging phenomenon degraded the device operation and lifetime severely. Extensive research has been carried out to identify the causes of aging and to seek viable solutions. Channel and substrate hot carrier injection

(HCI and SCI), channel hot electron/hole (CHE/H), drain avalanche injection, and radiation were found to be the main degradation mechanisms [25–31]. Hot carrier-induced degradation is of prime interest for designers as the process aggravates with downscaling. Degradation is essentially due to the enhancement of the electric field with dimension reduction, in the lucky electron model representation, providing the carriers enough energy to be injected through the oxide layer. These carriers are most likely to be captured by the existing oxide traps or to break the silicon bonds and thus giving rise to a localized and nonuniform pile-up of interface states near the drain–channel junction [32]. A energy-driven paradigm proposed by Rauch et al. suggests that the electron–electron scattering mechanism, governed by energy rather than the electric field, is responsible for aggravation of hot carrier degradation in downscaled devices [33].

The concept of junctionless transistor was proposed by Lee et al. [34] as a simple way to overcome process limitations. Indeed, as downscaling of channel lengths trends toward less than 10 nm, controlling process-induced variability becomes imperative to conserve the properties of transistors. At these scales, inherent scattering and diffusion of shallow-extension impurities into ultra-short channels pose a serious problem. As high doping concentration gradient is primordial, the extension formation with the actual process techniques implies additional complex and costly operations [35]. Contrary to IM MOSFETs, measurements highlighted an enhancement in the effective mobility with the increasing gate bias [36]. The enhancement is so significant that the effective mobility exceeds the corresponding bulk mobility especially in the accumulation regime [37]. Surface mobility also significantly improved in the accumulation layer of heavily doped devices, which indicates a higher current in the accumulation regime of the junctionless field-effect transistor (JLFET). This effect is attributed to the impact of the accumulation layer on screening of ionized impurities, yielding a reduction of Coulomb scattering [38]. In heavily doped devices, measurements highlight a correlation between the carrier density and the Coulomb scattering limitation, where a significant improvement in the effective mobility with respect to the carrier density is observed [39, 40]. Also, it was demonstrated that enhanced electrostatic controllability provided by multigates and thinner equivalent oxide thickness (EOT) yielded higher carrier density and improved mobility.

## 1.4 Study of Electrostatic and Dispersion Forces in Nanoelectromechanical Systems (NEMS)

Due to the outstanding electrical and mechanical properties of nanostructures, researchers are interested in novel generations of ultrasmall devices such as micro- and nanoelectromechanical systems (MEMS and NEMS, respectively), which are used in switches, actuators, sensors, AFMs, mass and force detectors, etc. New effects appearing due to the scale alteration in geometry introduce several additional terms into the theory of nanoscale structures, while their influence on other scales is negligible. One of these effects is dispersion forces. Dispersion

forces or quantum interactions, including the Casimir and van der Waals (vdW) regimes, play a key role in the behavior of nanodevices [41–43], related to the structure dimensions/configurations and the gap between electrically actuated electrodes [44]. The total electromagnetic Casimir energy is the sum of energies of the Dirichlet and Neumann modes. However, in large separations, the Dirichlet mode is dominant, while the Neumann mode is negligible [45]. It should be noted that the large separation assumption is valid for most real nano-tweezers since the gap between the arms is relatively larger than the radius of the arms ( $D \gg R$ ). Typically, for ( $D < 100R$ ), the contribution of the Neumann mode is negligible compared to the Dirichlet mode, and the asymptotic approximation provides an excellent estimation of the Casimir force [46]. In this section, practical mathematical models by assuming the large separation approximation (Dirichlet mode) are developed.

## 1.5 Nanomaterials for Wearable, Flexible, and Stretchable Strain/Pressure Sensors

Hardness and rigidity of micro and smart electronics cause mechanical deformation because of brittleness and inflexibility of their material components. This has restricted the application of non-flexible electronics that were replaced with electronic devices containing polymer and plastic substrates as flexible electronics in the past decades. In electronic devices, flexibility implies lightweight, elasticity, non-brittle, ductility, and easy fabrication [47]. Flexible electronics aroused great interest among researchers, industries, organizations, and military sectors to design and manufacture hybrid composite structures with lightweight flexible electronic devices [48]. On the other hand, the rapid growth of technologies, especially Internet in our daily life, has resulted in the advent of wearable technology in recent years [49]. Wearable and flexible sensors and biosensors have been widely explored in research and industry [50–52]. Sensors convert one form of energy into another form for processing [53]. Sensors detect environmental changes using conductive materials and send data to the computer for processing [54]. Conventional detection methods have been replaced by wearable and stretchable sensing electronics with nanomaterials [55]. Structures and designs of wearable sensors as well as nanomaterials determine sensor applications and their performance. Nanomaterials and nanocomposites depending on their properties, shape, size, structure, porosity, and fabrication method impart different sensor properties to wearable substrates. Strain/pressure sensors measure deformations, pressure stimuli, and mechanical properties [56, 57]. Metallic and semiconducting films were conventionally used as strain sensors and exhibited brittleness and rigidity with low stretchability [58]. These bulk materials could not attach to wearable substrates.

Nanomaterials including metal and metal-oxide nanoparticles and nanowires, conducting polymers (CPs), graphene, and CNTs have been explored due to their larger surface area compared to bulk materials. Superior mechanical and electrical properties and use of lower active materials are some of the advantages of the

integration of nanostructures and hybrid nanomaterials with flexible supports. The supports can also maintain their stretchability, wearability, and flexibility [59–64]. Flexible wearable piezoresistive strain/pressure sensors are composed of conductive sensing elements in addition to elastic polymers or other flexible/stretchable substrates. The contact resistance of the conductive part changes with strain/pressure stimuli, detected by electrical measuring systems. Different conductive nanomaterials have been explored as conductive fillers of elastomer composites including metal nanoparticles, nanowires and thin films, CPs, and carbon nanomaterials due to their desirable electrical and mechanical properties [65–71]. PDMS, polyurethane (PU), silicon rubber, Ecoflex, and Lycra are also explored as elastic substrates or components for conductive nanomaterials [72, 73]. On the other hand, incorporation of metallic nanomaterials, CNTs, and graphene with flexible wearable substrates propose desirable gauge factor ranges, introducing different structures and resulting in strains inside the matrix during stretching [74, 75]. Disconnection between nanomaterials decrease the contact area between them, leading to higher electrical resistance.

Graphene is another impressive carbon-based nanomaterial for resistance-based strain sensors due to its high electrical conductivity and mechanical properties [76–78]. Applied strain can change and partially destroy the hexagonal structure of the edges of graphene films [79]. Graphene can be combined with elastic polymers, which are generally grown through chemical vapor deposition or derived from exfoliated graphite. The shape and structure of graphene determine the flexibility and stretchability of sensors. To increase the stretchability and sensitivity of graphene in strain/pressure sensors, certain structures and engineering strategies were designed [80, 81]. In another work, macroscopic, flat, uniform graphene ribbons were fabricated through a modified wet spinning method [82]. Carbon black (CB) and graphite were also integrated with textiles to show piezoresistivity [83–85]. Natural biomaterials including natural textiles such as silk and cotton can be converted into conductive carbon materials via hydrothermal and pyrolysis processes [86, 87]. Carbonized silk nanofiber membranes integrated with PDMS film were also reported as skin-like pressure sensors.

## 1.6 Conductive Nanomaterials for Printed and Flexible Electronics Application

Printing is a process whereby formulated inks are deposited on the top of the substrate material for data transfer just as graphics, images, text, and the forms reappear as an image-carrying medium called substrate. Accordingly, printed and flexible electronics follow a set of printing methodologies to build electronic devices on flexible substrates. In the bubble-jet printing model, there is a print head with a heating unit. This heating unit is responsible for the preparation of ink bubbles and also forces the ink drop out of the nozzle. In the piezoelectric printing model, the nozzle

has a ceramic piezoelectric tile that gets expanded into the ink reservoir inside the print head and forces the ink drop out of the nozzle. The technology that enables to print inks on a variety of substrates with flexible or rigid structure materials is called screen printing. The entire process is relatively simple, flexible, and economical. The ink passes through a stencil made of a porous material during printing and gets deposited onto the substrate material. A delicate mesh made of nylon is used as a whole screen and stretched over a wooden or aluminum frame with a fitness of 150–400 fiber in.<sup>-1</sup>

A high-resolution printing technique that uses an electric field to produce an essential fluid flow for ink delivery onto a substrate is called an electrohydrodynamic printing. It produces two to five smaller droplets compared to the nozzle size. The positive impact on the shape regulation of nanoparticles in the droplets developed for printing is due to the electric field existing between the substrate and the nozzle. It is also preferred in 3D structure additive manufacturing. Magdassi et al. prepared concentrated citrate-reduced silver nanocolloids as ink for inkjet printing on surfaces such as glass and paper. The material was prepared by redispersion following lyophilization of newly prepared colloids. Carboxymethyl cellulose, a polymer stabilizer, was used as a binder and stabilizer. The material was characterized by its high electrical conductivity, reactivity, and optical properties [88]. Shankar et al. [89] synthesized Ag NPs by a reduction method using tin acetate as a reducing agent with a passivating shell of dodecylamine (DDA). This process was carried out in the toluene medium. The aim was to formulate nonaqueous conductive ink to print circuits for antennas and radio frequency identification (RFID) tags on surfaces such as Epson photo paper through aerosol jet printing. Lai et al. presented a review article on synthesis of silver NP and inks. Also, control of chemical concentration is significant to maintain the size and morphology of nanoparticles. The most suggested method to synthesize nanoparticles is chemical reduction, which requires a reducing agent to decrease the ion solution to the physical nanoparticle form. The authors concluded that most printing metal inks in the market are silver based owing to its remarkable electrical properties [90]. Zhou et al. performed a study on DDA-protected Ag NPs by modifying a small amount of dodecanethiol as the co-protective agent to formulate conductive silver ink for inkjet printing. The study revealed that electrical properties of silver can be enhanced quickly by heat treating at 90 °C, thus proving its suitability to print electronic circuits [91]. A similar team also synthesized water-dispersible Ag NPs using polyacrylic acid as a capping agent to inkjet print on paper substrates. Following the treatment of the Ag NPs with the poly(diallyldimethylammonium chloride) [PDAC] solution at room temperature, the nanoparticles coalesced together after the detachment of polyacrylic acid (PAA). The films showed changes in the morphology and electrical properties. Which is significant identification for printed electronic devices [92]. Zhang et al. synthesized Ag NPs for paper-based electronics through inkjet printing. Conductivity of the printed silver tracks was enhanced by a multiple-step room temperature (RT) post-processing method. Electrical properties, mechanical flexibility, and strain sensitivity of the material are proven effective to serve the 3D

electronics in future [93]. Kastner et al. and Shahariar developed Ag NPs for inkjet printing of conductive lines on textiles. The reactive silver ink contained silver in the complexed form, and no dispersions were found. The inkjet printer electronic circuit paths on the fabric were found to withstand washing tests, moisture, and heat [94, 95]. Liang et al. developed water-based Ag nanowires to fabricate wearable thin-film transistors and stretchable conductors through screen printing on polyethylene terephthalate (PET) sheets. A new water-based Ag nanowire ink was prepared using a mixture of (hydroxypropyl) methylcellulose, fluorosurfactant, distilled water (DI) as a solvent, and an antifoaming agent as an organic binder. Investigations were carried out to connect the rheological properties of the ink with its composition [96].

Patil et al. performed a study on inkjet printing of silver nanowires synthesized by the polyol method. The study focused on conductivity improvement printed pattern stability on flexible surfaces and techniques followed. The process was optimized by varying the concentration of isopropyl alcohol and the Ag nanowire mixture suspended in ethylene glycol, which was synthesized. The printed patterns obtained using the developed ink demonstrated high conductivity and strength [97]. Zhao et al. performed their study on selective dopamine determination in human serum using inkjet-printed multi-walled CNT chips. The CNT ink was examined with homogeneous double layers to increase the efficiency of dopamine detection. This method successfully resulted in the demonstration of the samples. The low-cost approach for the ink formulation paves a way for futuristic applications in printed sensors [98].

## 1.7 Metal-oxide Semiconductors for Noninvasive Diagnosis of Breast Cancer

In recent years, research in biomedical engineering has enabled clinicians to achieve early medical diagnosis with help of advanced technologies. Although these conventional diagnostic techniques help in diagnosis of cancer, they have certain drawbacks: high cost, painful to patients, and may not always give accurate results, especially in the early stage of the disease.

Recent research has revealed that the overall cost of cancer diagnosis and treatment is indeed decreasing for patients treated in the early stages; hence, the prognostic management of cancer remains a topic of key interest in the scientific community, from fabrication of devices to even machine learning [99]. Over the past few decades, advances in molecular biology and biotechnologies have achieved significant milestones to identify cellular changes at the molecular level, which may be a promising approach for early disease detection. Moreover, present technologies can quantify cellular changes at an early phase of disease development. This may help in identifying particular pathophysiological processes and underlying conditions to build more accurate devices [100–103]. The early diagnosis of cancer is crucial for patient survival; therefore, sensitive and specific methods are required for early cancer diagnosis. These methods aid clinicians in successfully diagnosing and treating patients, thus, increasing their chances of survival [104].

The conventional diagnostic methods for cancer detection involve histological characterization such as staining based on cell morphology and analyzing the slides using microscopic techniques. These are invasive techniques that require human sample collection by taking a biopsy sample followed by sample processing techniques that involve cell fixation and further analysis using a microscope to detect cancer cells [105–107]. Breast cancer is a result of interplay of various factors that lead to genetic mutations. Hereditary and environmental factors play a major role in causing these mutations, which inactivate the DNA repair genes in the breast cells [108]. The main biomarkers associated with targeted therapy of breast cancer are estrogen receptor and progesterone receptor. Growth factors such as epidermal growth factors, mainly ErbB-1 (EGFR) and ErbB-2 (ERBB2, HER-2/neu, HER2), are also regulated in breast cancer tumorigenesis [109, 110]. EGFR overexpression is correlated to overexpression of HER-2, levels of which are used for targeted therapy by using the drug trastuzumab [111]. However, breast cancer type is classified based on gene expression profiling, which requires a large amount of tumor tissue for analysis and is highly expensive and also a difficult procedure. Moreover, gene expression in an individual is subject to changes due to post-transcriptional modifications and may lead to upregulation or downregulation of certain genes [112]. The diagnosis of breast-cell-related diseases requires an extensive biopsy and sampling for confirmation. These invasive diagnostic techniques cause distress until the diagnosis is confirmed through biopsy, and sometimes even after treatment there is a high chance of relapse; therefore, the patient has to get a biopsy done every few months. Some benign tumors, such as premalignant hyperplasia, when left untreated can also lead to invasive breast cancer, which is one of the most common malignancies diagnosed in women.

Breath analysis is widely being explored as a noninvasive diagnostic test for detection of breast cancer [113]. Increased oxidative stress is a key factor regulated in breast cancer, which causes damage to the cellular DNA, lipids, and proteins. Also, cytochrome P450 enzyme, expressed in breast cancer, causes lipid peroxidation of polyunsaturated fatty acids and leads to overexpression of volatile organic compounds such as alkanes and alkane derivatives in breath [114, 115]. Apart from lipid peroxidation, free radical-induced oxidation of certain amino acids, proteins, and peptides has also produced hydrocarbons and monoaldehydes [116, 117]. Recently, implementation of optical fibers in sensor application is rapidly increasing due to their ease of fabrication, low cost, and immunity to electromagnetic interferences. Especially in volatile organic compound (VOC) gas sensor applications, optical fibers are widely used because of their fast response and sensitivity toward gas molecules. Different types of optical fibers have been reported in sensor applications such as plastic optical fibers, silica optical fibers, fiber Bragg grating optical fibers [118], photonic crystal optical fibers [119]. In addition to the geometry and types of optical fibers, various sensing mechanisms have been reported, including absorption-based sensors, evanescent mode [120], plasmonic mode optical sensors such as surface plasmon resonance [121], localized surface plasmon resonance [122], and lossy mode resonance [123].

## 1.8 Down-conversion Photoluminescence Properties of $\text{ZrO}_2:\text{Ln}^{3+}$ ( $\text{Ln} = \text{Eu, Sm, Er, Tb, Ho, Tm, Pr, Gd, Dy}$ ) Films Formed by Plasma Electrolytic Oxidation

In recent years, plasma electrolytic oxidation (PEO) is a very convenient process for formation of Ln ion-doped metal-oxide semiconductor films such as  $\text{ZrO}_2$  [124–132],  $\text{Al}_2\text{O}_3$  [133–139],  $\text{TiO}_2$  [140, 141],  $\text{Zn}$  [142],  $\text{Nb}_2\text{O}_5$  [143],  $\text{HfO}_2$  [144],  $\text{Y}_2\text{O}_3$  [145], and  $\text{Gd}_2\text{O}_3$  [146] by PEO of pure Zr, Al, Ti, Zn, Nb, Hf, Y, and Gd metals, respectively, in an electrolyte containing suitable lanthanide oxide ( $\text{Ln}_2\text{O}_3$ ) particles. The formation mechanism of the PEO film is complex, as it involves electro-, thermo-, and plasma-chemical reactions in the electrolyte and metal–electrolyte interface, due to locally high temperature ( $10^3$ – $10^4$  K) and pressure ( $\sim 10^2$  MPa) at the micro-discharge sites [147].

During the PEO process of zirconium in an alkaline electrolyte containing  $\text{Ln}_2\text{O}_3$  particles,  $\text{ZrO}_2$  films are formed by PEO as a result of the oxidation of zirconium substrate via a sequence of localized micro-discharging events.  $\text{Zr}^{4+}$  ions formed at the zirconium/oxide interface ( $\text{Zr} \rightarrow \text{Zr}^{4+} + 4\text{e}^-$ ) enter the micro-discharge channels and react with  $\text{O}^{2-}/\text{OH}^-$  ions from the electrolyte. Metal oxides are eminent host matrices for  $\text{Ln}^{3+}$  due to their outstanding physicochemical characteristics such as good thermal, chemical, and physical stability, wide bandgap, broad optical transparency, low phonon frequency. Among them, zirconium oxide (zirconia,  $\text{ZrO}_2$ ) is an excellent host material because its low phonon energy of about  $470\text{ cm}^{-1}$  can increase the probability of radiative transition occurrence and reduce non-radiative multiphonon relaxation of excited  $\text{Ln}^{3+}$  throughout the vibrational bands of the  $\text{ZrO}_2$  host lattice, thus foreseeing a high yield of intra-4f transitions from the  $\text{Ln}^{3+}$  [148–150].

The  $\text{Ln}_2\text{O}_3$  particles take part in PEO process through the electrophoretic and micro-discharging mechanisms [151].  $\text{Ln}_2\text{O}_3$  particles have a negative zeta potential in alkaline media; thus, its particles are negatively charged. Due to the electrophoretic effect, the  $\text{Ln}_2\text{O}_3$  particles move toward the zirconium anode. Melting point of  $\text{Ln}_2\text{O}_3$  particles ( $\sim 2400^\circ\text{C}$ ) is much lower than locally high temperatures ( $\sim 7000^\circ\text{C}$ ) which induced at the micro-discharging sites [152], allowing the molten  $\text{Ln}_2\text{O}_3$  particles to react with  $\text{ZrO}_2$  and form  $\text{Ln}^{3+}$  ion-doped  $\text{ZrO}_2$  films.

## 1.9 Multiferroics for Spintronic Applications

Multiferroics are a special class of materials that simultaneously possess two or more primary ferroic order parameters in the same phase such as ferroelectricity, ferromagnetism, ferroelasticity, and ferrotoroidicity [153]. In the last few decades, a significant number of research works have been done on multiferroics. A material that simultaneously possesses multiferroic orders is not sufficient. There should be a strong coupling interaction between different orders to achieve potential applications. Magnetoelectric coupling refers to the linear magnetoelectric effect [154]. One

- hot carrier degradation (HCD) 97  
 creation process 104–108  
 degradation of 108–118  
 simulation framework of 102–103  
 static analysis 118–119  
 transient analysis 119–121
- hot carrier injection (HCI) 97
- Hummer's method 29
- hybrid nanogenerators 75, 76
- hydrothermal method 67
- i**
- immunosensor 36
- impedometric methods 33
- indium-tin-oxide (ITO) 30
- Inelastic Electron Tunneling Spectroscopy (IETS) 307
- inkjet printing 209
- integrated electrode (IDE) 35
- inverse direct gravure printing 211
- j**
- JLFET 98
- Judd-Ofelt analysis 281
- Julliere's model 304
- k**
- Klaassen mobility model 102
- l**
- laser ablation 225
- laser beam pulse 67
- Lennard-Jones potential 139
- li-ion battery 31
- line edge roughness (LER) 100
- liquid-phase synthesis 67
- lossy mode resonance (LMR) 263
- m**
- magnetic dipole transition 284
- magnetic tunnel junction (MTJ) 12, 304
- magnetoelastic effects 301
- magnetoelectric (ME) effects 301
- magnetoelectric coupling 301, 305
- magnetoresistance 302
- mammography 250
- mass-selected ion injected 258
- mechanochemistry method 66
- Mejis-Fokkema model 136, 137
- metal oxide semiconductors 8, 10
- metallic based inks 214–215
- micro-electromechanical systems (MEMS) 4
- microcantilever 319
- microfabricated tuning fork 13, 331
- Miller capacitance 121
- molecularly imprinted polymers (MIPs) 336
- MOSFET  
 reliability-based analysis 3–4  
 junctionless transistor 98–102  
 creation process 104–108  
 degradation of 108–118  
 hot carrier degradation 102–103
- multiferroic materials 11–12  
 magnetoelectric materials 301, 302  
 spintronics 302
- multiferroic tunnel junctions (MFTJs) 307–309
- multiple electrospun wires 13, 340
- multiple ion monitoring mode 258
- n**
- nano-electromechanical systems (NEMS) 4–5  
 electrostatic forces 137  
 Casimir forces 141–149  
 electrostatic forces 131  
 freestanding phenomenon 149–151  
 van der Waals forces 137–141
- nano-electronics biosensors 1, 2
- nanoelectronics 30
- nanogenerator (NG) 3, 71  
 hybrid 75–76  
 piezoelectric nanogenerators 71–72  
 pyroelectric 74–75  
 triboelectric nanogenerators 73–74
- nanomaterials 5–6, 30  
 based inks 213–215  
 growth 255–257

- needle–wire connections 69  
 noise margin (NM) 118  
 non-enzymatic glucose biosensor 40, 41
- O**
- Ohnesorge number 209  
 organic multiferroic tunnel junctions (OMFTJs) 308  
 oxide trapping/detrapping process 105
- P**
- Palmer's model 136  
 piezoelectric nanogenerators (PENGs) 71–72, 76–79  
 piezoelectric printing model 7, 209  
 piezomagnetic effects 301  
 plasma electrolytic oxidation (PEO) 10, 280  
 polarized neutron reflectometry (PNR) 11, 303  
 polyacrylamide (PAM) 335  
 polyacrylic acid 8  
 polybutadiene 334  
 polycrystalline graphene 1, 27–28  
 polymer film bridges 338–342  
 polymer wire bridges 331–338  
 polymethyl methacrylate (PMMA) 340  
 polystyrene (PS) 329  
 polyvinylcinnamate (PVCN) 13  
 polyvinylpyrrolidone (PVP) 338  
 potentiometric methods 33  
 printable nanomaterials 212  
 printed electronics (PE) 207  
 pristine graphene 1, 27  
 proton transfer reaction mass spectrometry (PTR-MS) 258  
 proximity force approximation (PFA) 144–148  
 pulsed laser deposition (PLD) 255  
 pyroelectric nanogenerators 74, 75
- Q**
- QR codes 338  
 quantum confinement effect 101  
 quantum mechanical effect 303  
 quartz crystal microbalance (QCM) 319  
 quartz enhanced photo-thermal spectroscopy (QEPTS) 321  
 quartz enhanced photoacoustic spectroscopy (QEPAS) 321  
 quartz tuning fork (QTF) 12–13  
   chemical sensors 318–324  
   early development 324–325  
   mass loaded sensor 328–331  
   modified with polymer film bridges 338–342  
   modified with polymer wire bridges 331–338  
   sensor 325–329  
 quick response (QR) codes 338
- R**
- rectangular beam-sheets 138  
 reduced graphene oxide (RGO) 1, 27, 28  
 resonant frequency 321  
 roll-to-roll (R2R) printing 212
- S**
- scanning electron microscope (SEM) 66, 281, 337  
 Schottky contact 3  
 screen printed electrode (SPE) 35  
 screen printing 7, 210  
 selected ion flow tube-mass spectrometry (SIFT-MS) 257–258, 337  
 semiconductor metal oxide (SMO) 252  
 shaft tweezers models 130  
 silver nanoparticles 215–222  
 silver nanowire 222–226  
 SiO<sub>2</sub>, graphitization of 27  
 slot die coating 210–211  
 sol-gel synthesis 66–67  
 spin-dependent tunneling (SDT) 304  
 spin FET 309–311  
 spin LED 311  
 spin orbit coupling (SOC) 311  
 spin valve 306–307  
 spin-transfer torque (STT) 308

- spin-orbit torque field effect transistor (SOTFET) 311
- spintronics  
 fundamental aspects of 302–303  
 giant magnetoresistance 303  
 multiferroic tunnel junction 307–309  
 spin FET 309–311  
 spin LED 311  
 spin valve 306–307  
 tunneling magnetoresistance 304
- spray pyrolysis (SP) 255
- Stokes shift 279
- substrate carrier injection (SCI) 97
- supercapacitors 30
- surface plasmon resonance (SPR) sensor 264–265
- t**
- Taylor series expansion 134
- Tedlar sampling 337
- thermally assisted switching (TAS) 308
- thick film deposition 255
- thin film deposition 252–254
- threshold voltage 118
- Tragacanth gum 68
- transconductance 97, 110, 111
- triboelectric nanogenerators (TENGs) 73–74
- tunneling magnetoresistance (TMR) 304
- u**
- ultrasonic irradiation 67
- ultrasound 250
- up-conversion PL 279
- v**
- Van der Waals force 137  
 carbon nanotubes (CNT) tweezers 140–141  
 carbon nanotubes (CNT)-sheets 138–139  
 circular tweezers 140  
 rectangular beam-sheets 138  
 rectangular tweezers 139–140  
 wire plate 138
- vapor transport synthesis 68–69
- vapor-liquid solid (VLS) method 3, 70
- volatile organic compound (VOC)  
 body metabolism for 247–249  
 evanescent wave fiber optic sensors 263  
 lossy mode resonance fiber optic sensors 263–264  
 breast cancer related 250  
 components of human breath 249  
 composite metal oxides for 252  
 sensing, metal oxides for 252
- voltage transfer characteristic (VTC) 118
- voltammetric methods 33
- w**
- wet-chemical method 2
- wet spinning method 6
- x**
- X-ray diffraction (XRD) 66, 281
- X-ray energy dispersive spectroscopy (EDS) 281
- z**
- zinc nitrate hexahydrate 2
- zinc oxide (ZnO)  
 controlled precipitation 67–68  
 hydrothermal method 67  
 liquid-phase synthesis 67  
 mechanochemical method 66  
 NPs crystal structure of 63–66  
 piezoelectric effect 69–70  
 piezoelectric nanogenerators 70–79  
 structure of 63  
 sol-gel synthesis 66–67  
 vapor transport synthesis 68–69  
 wurtzite-structure of 72
- zinc oxide piezoelectric nanogenerators 3

- ZrO<sub>2</sub>
- chemical and phase composition
    - 281–283
  - Dy<sup>3+</sup> 292–293
  - Er<sup>3+</sup> 286
  - Eu<sup>3+</sup> 283–285
  - experimental 280–281
  - films 283
  - Gd<sup>3+</sup> 292
  - Ho<sup>3+</sup> 288
  - Ln<sup>3+</sup> 295
  - morphology
    - 281–283
  - Pr<sup>3+</sup> 290–292
  - Sm<sup>3+</sup> 286
  - Tb<sup>3+</sup> 287–288
  - Tm<sup>3+</sup> 288–290
  - undoped 283